Available online at www.sciencedirect.com
ScienceDirect
Journal of the European Ceramic Society 28 (2008) 1749–1762
www.elsevier.com/locate/jeurceramsoc

Evolution of aluminosilicate structure and mullite crystallization from homogeneous nanoparticulate sol–gel precursor with organic additives

Jarkko Leivo [a,*], Mika Lindén [b], Jessica M. Rosenholm [b], Merja Ritola [a], Cilâine V. Teixeira [b], Erkki Levänen [a], Tapio A. Mäntylä [a]

[a] *Department of Materials Science, Tampere University of Technology, 33101 Tampere, Finland*
[b] *Department of Physical Chemistry, Åbo Akademi, 20500 Åbo, Finland*

Received 20 July 2007; received in revised form 5 December 2007; accepted 9 December 2007
Available online 4 March 2008

Abstract

The influence of non-ionic polyethylene glycol and poly(vinylpyrrolidone) on monophasic-like nanoparticulate aluminosilicate with mullite bulk composition was investigated. The chemical homogeneity in the sol–gel state, as well as the evolution of the calcined aluminosilicate/mullite structures thereof, was studied by dynamic laser scattering, small angle X-ray scattering, nuclear magnetic resonance spectroscopy, X-ray diffraction, differential thermal analysis, dilatometry, N_2 adsorption and Fourier transform infrared spectroscopy. The results show that the organic additives have virtually no influence on the chemical structure of the monophasic-like nanoparticles in the sol–gel state, and the overall homogeneity of monophasic gels in the fired ceramics was generally sustained, as judged by the Type I crystallization. The porosity was not due to the polymers directly acting as porogens, but due to voids formed during the restructuring of matter during heat treatment.

Keywords: Sol–gel processes; Inclusions; Mullite; Nanoparticulate aluminosilicate

1. Introduction

High-purity aluminosilicates with mullite bulk composition, $Al_2^{VI}[Al_{2+2x}^{IV}Si_{2-2x}]O_{10-x}$, are interesting materials for use in optical[1] and electrical[2] components, as well as thin films for separation and purification membranes,[1] porous coatings[3] and candidates in biological coatings for osteoblasts.[4] Typically, the performance is crucially dependent on the homogeneity of the aluminosilicate phase, and a distinct crystallization of the transitional Al-rich mullite at temperatures below 1000 °C is believed to indicate high level of precursor homogeneity.[5–15] The most homogeneous precursor sols, frequently denoted Type I,[7–11] are prepared by sol–gel processes, which, however, are often time-consuming and/or the sols may not be stable over time. Mismatches in hydrolysis kinetics or low sol stability may induce heterogeneous regions within the gel (then denoted Type III precursor),[7–9] leading to the formation of an intermediate spinel phase at ∼1000 °C.[16]

We have recently described a fast and an easy method for preparation of a homogeneous aluminosilicate/mullite high-purity precursor (of Type I) in the form of nanoparticles in a water-based sol that can remain stable for years.[17] The sol consists of partially hydrolysed 2 nm hydroxy-alkoxo-aluminosilicate nanoparticles, structurally closely resembling a proto-imogolite allophane phase (PI/A), which crystallizes into a nanocrystalline transitional mullite with no spinel phase formation. The gel can easily be re-dispersed if dried at room temperature, indicating that interparticulate condensation reactions are slow. Inspired by our recent findings that porous, chemically homogeneous aluminosilicate films are good substrates for cell growth,[4] where the porosity was induced by addition of hydrogen-bonding polymers, we have performed a more detailed study on the influence of the added polymers on the sol structure as well as on the phase purity of the ceramics. For high-purity mixed oxide materials, non-ionic organic

* Corresponding author. Current address: Millidyne Oy, Hermiankatu 6-8 G, 33720 Tampere, Finland. Tel.: +358 50 322 64 55; fax: +358 3 317 79 00.
E-mail address: jarkko.leivo@millidyne.fi (J. Leivo).

0955-2219/$ – see front matter © 2008 Elsevier Ltd. All rights reserved.
doi:10.1016/j.jeurceramsoc.2007.12.033

additives that can stabilize (or destabilize, i.e., flocculate) particulate sols, for example, poly(ethylene glycol), PEG, poly(vinyl pyrrolidone), PVP, and mixtures of these, are often used as structural modifiers and sol–gel processing aids.[18–21] During processing, the chemical homogeneity of sols may be influenced by the presence of residual hydroxyls and organics,[22] chelating agents,[23] and additional salts and counter-ions.[12,24] Of our special interest is the interplay between phase purity and aluminosilicate porosity with hydrogen-bonding polymers, as compositions yielding homogeneous aluminosilicate phase with or without transitional mullite crystals showed the best biocompatibility. For sol–gel-derived biomaterials, it is known that in the presence of transitional ceramic phases or pores, especially when the pore sizes are in the mesoporous range (2–50 nm), the bone response for biomaterials can be enhanced.[25–27]

In this paper, we investigated the evolution of nanoparticulate aluminosilicate structure containing PEG, PVP or their mixture. The effect of chloride was studied, as chloride is also a common counter-ion for many surfactants and water-soluble polymers. However, it is also known that chloride may interfere with the aluminosilicate phase homogeneity and the formation of mullite thereof.[24,28,29] Additionally, for water-based thin films, the sol viscosity and surface tension can be modified by an addition of suitable co-solvents, such as 1-propanol, and therefore also 1-propanol/water mixed solvent systems were studied. Several characterization methods were used; dynamic light scattering and small angle X-ray scattering were used for particle size determinations in sols, the chemical structure of nanoparticles in gels was determined by solid-state ^{29}Si and ^{27}Al nuclear magnetic resonance spectroscopy, differential thermal analysis was used for the characterization of thermal events during the heat treatment, the crystallinity, the chemical structure, and the porosity of calcined materials were determined by X-ray diffraction, Fourier transform infrared spectroscopy and N_2-sorption analysis, respectively, and the shrinkage during heat treatment was determined by dilatometry.

2. Experimental procedure

2.1. Sample preparation

All of the studied sol compositions are listed in Table 1. The nanoparticulate sol M0 was synthesized from a water-based alkoxide solution of $Al(NO_3)_3{\cdot}9H_2O$ (ANN; ≥98.0%), $Al(O^iC_3H_7)_3$ (AIP; +98%) and $Si(OC_2H_5)_4$ (TEOS; 99%) following a modified Nishio–Fujiki method[6] as described by Leivo et al.[17] Briefly, the source chemicals were dissolved in 95 mol of deionised water with the total molar composition 0.75:2.25:1.00 of ANN:AIP:TEOS, which corresponds to a n_{Al}/n_{Si} ratio of 3 found in 3:2-mullite, $3Al_2O_3{\cdot}2SiO_2$. The sol was stirred for 1 day at room temperature followed by ageing for 4 days under reflux at 60 °C. The so-prepared sol, denoted as M0 hereafter, was let to cool down to room temperature, and 100 g aliquots of M0 were withdrawn. Additives were then mixed into the aliquots in the respective order and amounts given in Table 1. After each ingredient addition, the sol was stirred for 1 h before potential subsequent additions of ingredients. Some sols void of mullite precursors were also

Table 1
Composition and pH of nanoparticulate sols

Sol	Additives mixed with M0 (100 g)	Additives (g)				pH	
		PEG	PVP 5%	3 M HCl	1-PrOH	Sol	Media
Sols							
M0	Sol without any additives					3.0	3.0
MG	PEG	2.5				3.0	3.0
MV	PVP		70			3.3	3.5
MVG	PVP and PEG	2.5	70			3.3	3.5
Sols with HCl							
M0h	HCl			2.5		2.7	0.9
MGh	PEG and HCl	2.5		2.5		2.7	0.9
MVh	PVP and HCl		70	2.5		3.2	1.1
MVGh	PVP, PEG and HCl	2.5	70	2.5		3.2	1.1
Sols with 1-PrOH							
MOP	1-PrOH				159	2.7	3.7
MGP	PEG and 1-PrOH	2.5			159	2.7	3.7
MVP	PVP and 1-PrOH		70		159	3.1 (spnt)[a]	4.1
MVGP	PVP, PEG and 1-PrOH	2.5	70		159	3.2 (spnt)[a]	4.2
Sols with HCl and 1-PrOH							
M0hP	HCl and 1-PrOH			2.5	159	2.5	1.7
MGhP	PEG, HCl and 1-PrOH	2.5		2.5	159	2.5	1.6
MVhP	PVP, HCl and l-PrOH		70	2.5	159	2.9 (spnt)[a]	1.8
MVGhP	PVP, PEG, HCl and 1-PrOH	2.5	70	2.5	159	2.9 (spnt)[a]	1.7

Sols that formed instant gels with white flocculants (*) were withdrawn from the further process. PEG, polyethylene glycol (M_w = 400); PVP, poly(vinylpyrrolidone) (M_w = 1.3 M) in 5% solution (aq.). Media indicates the reference media without nanoparticles, prepared separately from $NaNO_3$, 2-PrOH, EtOH and HNO_3, with corresponding polymer, salt and solvent amounts to the parent sol.

[a] Gelation with white flocculants; spnt, pH value of the supernatant.

prepared for reference purposes (media in Table 1). In these cases, the pH value was tuned to 3.0 by addition of 68% HNO_3 solution. Then, the additives were mixed into these solutions, with the corresponding amounts to the parent sols.

Nanoparticulate gels were prepared by evaporation in an open container for at least 1 week at room temperature. Once clear gels were formed, the gels were further dried overnight at 60 °C. The low drying procedure was chosen to avoid chemical gelation and complete removal of alcoholic species in order to maintain the original nanoparticle structure in the gels. The gels were crushed carefully before further processing. Discrete specimens of each of the gels were heat-treated either at 700 °C, 800 °C, 900 °C or 1000 °C with a heating rate 5 °C min^{-1}, with a dwell-time of 1 h. Additionally, gels were heated to 200 °C, 350 °C, 460 °C, 700 °C or 900 °C with a heating rate 5 °C min^{-1} and analysed by Fourier transform infrared spectroscopy.

2.2. Material characterization

Small angle X-ray scattering (SAXS) measurements were performed using a Kratky compact camera (Hecus, Graz, Austria) equipped with an X-ray generator (Model ID-3003, Seifert, Massillon, OH, USA) operated at maximum of 50 kV and 40 mA with Cu Kα radiation and a position-sensitive detector (Model 50 M, MBraun GmbH, Garching, Germany) covering a range of 0.5–8°. Measurements were performed in vacuum and corrected for the scattering of the capillary with solvent.

Dynamic light scattering (DLS) measurements were performed at 20 °C using a zetasizer equipment (Model Nano ZS, Malvern, Worcestershire, UK) fitted with a "red" laser operating at 632.8 nm and the detector positioned at 173° (non-invasive back scattering). The data was analysed using the Malvern Dispersion Technology Software v. 4.20 using the volume particle size distribution peak.

The ^{27}Al and ^{29}Si MAS NMR spectra were recorded with a 4-mm MAS probe on a spectrometer (Model Avance 500WB, Bruker, Billerica, MA, USA) operating at 130.37 MHz and 99.36 MHz, respectively. The experimental conditions for ^{27}Al NMR were a spinning rate of 15 kHz, a recycle delay of 1 s (2000 scans), and a $\pi/12$ pulse of 0.6 μs. Those for ^{29}Si NMR were a spinning rate of 10 kHz, a recycle delay of 10 s (7200 scans), and a $\pi/2$ pulse of 2.2 μs. The chemical shifts were referenced to $Al(H_2O)_6^{3+}$ for ^{27}Al and to pure tetramethylsilane for ^{29}Si.

Thermogravimetric analysis (TG) and differential thermal analysis (DTA) were carried out by using a thermal analysis instrument (Model STA 409, Netzsch, Burlington, MA, USA) under a flow of purified air (75 cm^3/min) with a heating rate of 5 °C min^{-1}.

Crystallization of mullite was studied by using X-ray diffraction (XRD), and patterns were recorded on a X-ray diffractometer (Model Diffrac 500, Siemens, New York, NY, USA) operated at 40 kV and 30 mA using Cu Kα radiation with a step time 1.2 s/step and a scan step 0.02° within the 2θ range of 5–80°.

Shrinkage was determined by using a dilatometer (Model DI-24, Adamel Lhomargy, Roissy en Brie, France) under a flow of purified air (75 cm^3/min) with a heating rate of 5 °C min^{-1}.

The specific surface areas (SSAs) were measured by the BET method from samples activated for over 12 h under vacuum at 300 °C using a gas sorption analyser (Model Omnisorp 100CX, Coulter, Hialeah, FL, USA) with N_2 at 77 K. The micropore volume was determined by the Lippens–deBoer *t*-plot method[30] and the mesopore sizes were calculated by applying the Barrett–Joyner–Hallender method[31] to the desorption branch of the isotherms.

Fourier transform infrared (FTIR) absorbance spectra were measured by a spectrometer (Model Spectrum One, PerkinElmer, Norwalk, CT, USA) using KBr pellets with 32 scans/sample and a resolution of 2 cm^{-1}.

3. Results and discussion

3.1. Sol characterization

As prepared, transparent sols were characterized by SAXS in order to determine the particle size. Representative Guinier plots of two extreme cases with respect to the type and amount of additives, as compared to M0,[17] are presented in Fig. 1. The radii of gyration, R_g, were calculated from Guinier plots and presented in Table 2. The R_g values obtained for the M0 sol and for corresponding sols containing polymers were in the range of 0.8–0.9 nm, which correspond to a particle diameter of 2.1–2.3 nm ($R_g = (3/5)^{0.5}R$).[32] This is the same particle size as that in M0.[17] In the presence of HCl, however, the particle diameters were generally about 3.1 nm, except for MVGh, for which particle size of 2.2 nm were observed. For sols containing both 1-PrOH and HCl, the corresponding values were 3.9–4.7 nm (the order of HCl–1-PrOH addition was found irrelevant). It is known that the adsorption of both PEG and PVP onto positively charged alumina is very limited and independent of pH.[33,34] The adsorption of Cl^-, on the other hand, may be fairly strong at pH

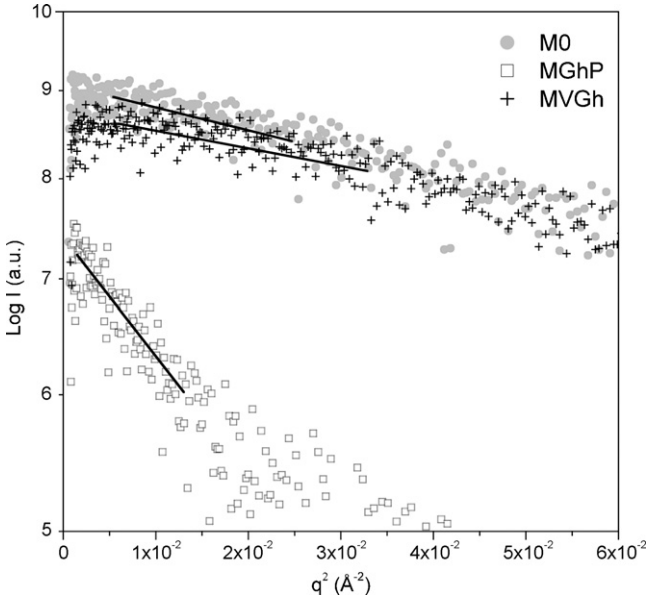

Fig. 1. SAXS Guinier plots of two sols with additives, MVGh and MGhP, as compared with the sol without any additives, M0[17].

Table 2
The radius of the gyration of nanoparticulate sols

Abbreviation	R_g (nm)
Sols	
M0	0.81 ± 0.14
MG	0.77 ± 0.14
MV	0.86 ± 0.15
MVG	0.89 ± 0.14
With HCl	
M0h	1.21 ± 0.11
MGh	1.23 ± 0.11
MVh	1.20 ± 0.15
MVGh	0.86 ± 0.01
With 1-PrOH	
M0P	1.56 ± 0.11
MGP	1.71 ± 0.12
With HCl and 1-PrOH	
M0hP	1.52 ± 0.06
MGhP	1.86 ± 0.02

values below the IEP,[35,36] which could partly explain the larger particle diameters measured in the presence of HCl. Also polymers like PEG are known to dehydrate in the presence of Cl^-, which may be another contribution to the R_g values measured for the polymer-containing sols. A possible alcoholysis in the presence of 1-PrOH addition,[37] may also lead to an increased particle diameter, and could enhance the adsorption of polymers onto the particle surfaces.

Dynamic light scattering measurements performed on the same sols yielded hydrodynamic particle diameters around 2 nm for the M0 sol, while the particle diameter in the MG sol was 3 nm. For PVP-containing sols, a much larger mean particle size of 40 nm was obtained. In both cases, similar particle sizes were obtained for corresponding sols, which did not contain any aluminosilicate particles, why it seems clear that these particles are polymer aggregates in solution. The smaller particle sizes obtained by SAXS as compared to DLS can be understood, as SAXS is more sensitive to the aluminosilicate particles, due to the high electron density contrast between the solvent and the particles. The addition of PEG to PVP-containing sols did not alter the particle size. However, in the presence of HCl, smaller diameters of 35 nm were detected, which indicates that chloride ions partly dehydrate the hydrophilic polymers making them form more condensed aggregates.

Solid-state ^{27}Al and ^{29}Si MAS NMR measurements were carried out on selected dried gels. Results obtained for two examples, M0 and MVGh, representing extreme cases in the studied compositional space, are shown in Fig. 2. The results obtained are almost identical. The major shift in the ^{29}Al MAS NMR measurement was approximately at 6.0 ppm (5.7 ppm for M0),[17] and the major shift in the ^{27}Si MAS NMR at around −78.5 ppm (−78.9 ppm for M0),[17] including two minor signals centred at −85 ppm and −90 ppm. The MAS NMR resonances, altogether, were assigned to oligomeric, not completely hydrolysed, nanoparticle structure of octahedrally coordinated (AlO_6) alumina and silica, whose silicon is mostly bond to one OH and three AlO_6.[12–15] A small portion of free trivalent $[Al(H_2O)_6]^{3+}$ aquo-ions might be present in both nanoparticulate gels, which is supported by the ^{29}Al MAS NMR results that displayed a knee at 0 ppm, which was present also in the M0 gel.[17] Thus, the results suggest that the chemical structure of the nanoparti-

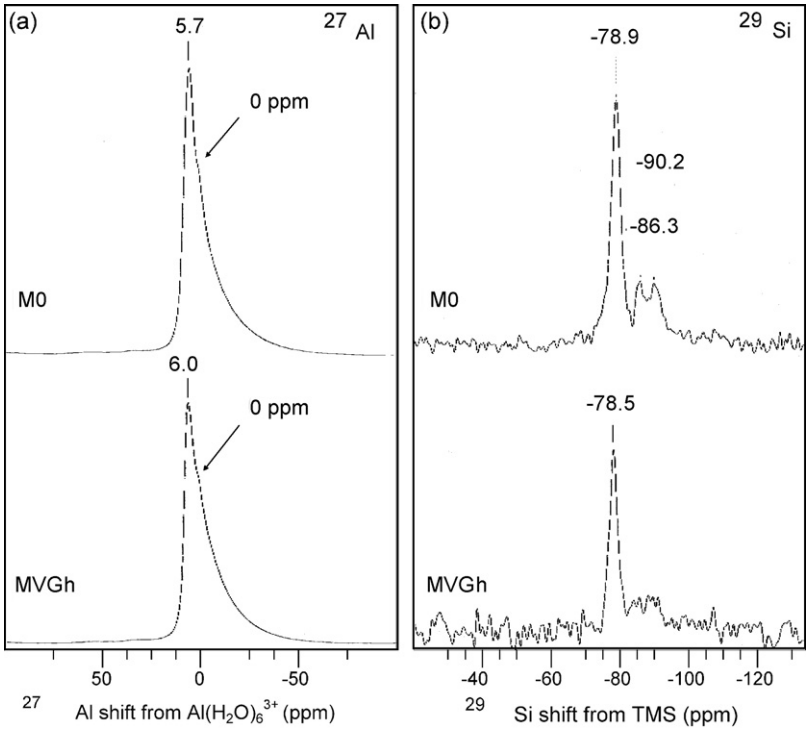

Fig. 2. (a) ^{27}Al MAS NMR and (b) ^{29}Si MAS NMR spectra of 60 °C dried non-added gel (M0) and PVP–PEG–HCl added gel (MVGh). The results of M0 are reproduced from the previous reference.[17]

cles is similar in both cases, within the limit of the resolution of solid-state NMR.

3.2. Transitional mullite and spinel phase crystallization

Heat-treated gels were characterized by XRD. All gels were X-ray amorphous at temperatures below 800 °C. XRD diffractograms for gels calcined at 900 °C and 1000 °C are presented in Fig. 3. At 900 °C, mullite was detected clearly for M0 and generally for gels that originally did not contain any polymer, while the polymer containing gels were amorphous. The exceptions were M0hP (without polymer no mullite) and with polymer MGP (with polymer very weak mullite). At 1000 °C, gels expressed clear transitional mullite reflections. However, an evident co-crystallized spinel phase was observed for MVGh.

The typical crystallization of transitional mullite, similar to Type I gels for the sol–gel-derived mullite,[7–11] indicates molecular homogeneity in all gels. Mullite crystallization at temperatures around 900 °C can be related to the earlier formation of mullite nucleation sites,[11,38] as kinematically mullite crystallizes by the nucleation process below 965 °C.[39] This suggests that the polymer containing gels were, in general, lacking of the early nucleation sites, indicating that mullite at 1000 °C crystallized via nucleation growth process that involved a diffusion of silicon atoms.[7,39] This was not generally inducing any heterogeneities, as the spinel phase was typically not observed. However, when both PEG and PVP were present in the sol together with the presence of HCl, the co-formation of the spinel phase was favoured. Interestingly, gels with PEG or PVP alone with or without HCl, did not show that evident formation of a spinel phase. It is known that if alumina is segregated, only a small amount of free alumina is sufficient enough to yield the spinel phase to dominate the crystallization at around 1000 °C.[16] In the case of free silica,[15] the Al-rich aluminosilicate regions and the modified short-range order may favour the formation of spinel phase (>75% alumina).[40] We note that the solid-state NMR data was similar for MVGh and for M0, which suggests that the formation of the spinel phase is not directly linked to alumina segregation or other atomic arrangements in the aluminosilicate nanoparticles in the sol–gel state, but to events occurring during the thermal treatment, most probably due to a pre-microphase separation where silica species are adsorbed to phase separated polymer together with Cl^- ions. Precursor systems with chloride are reported to show lower incorporation of non-bonded aluminium into the silica gel network than in the ones with nitrate,[28] and chloride ions can also remain in aluminosilicate gels at higher temperatures.[29]

3.3. Thermal analysis

The mass losses for each gel were high (Fig. 4a), as expected due to the low drying temperature. In the region of water desorption below 200 °C, a smooth loss curve was observed for the gels without polymers, while for the polymer containing gels (the PEG–HCl-containing gels as exceptions), a steep step in the mass loss curve was observed at 110–150 °C. Similar

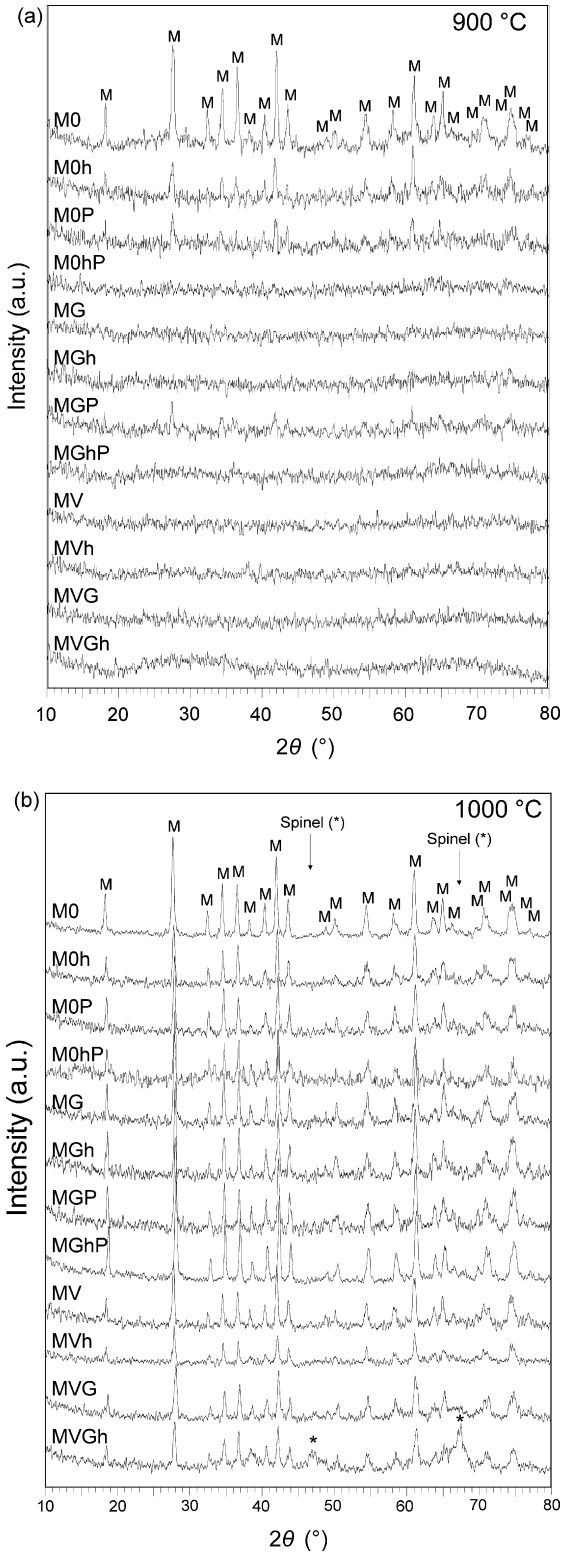

Fig. 3. XRD curves of samples heat-treated by using heating rate of 5 °C min^{-1} for 1 h at (a) 900 °C and (b) 1000 °C. All distinguishable peaks belong to mullite (M) of JCPDS reference file no. 73–1389, except Spinel (*) labelled for spinel phase, pronounced with the gel MVGh.

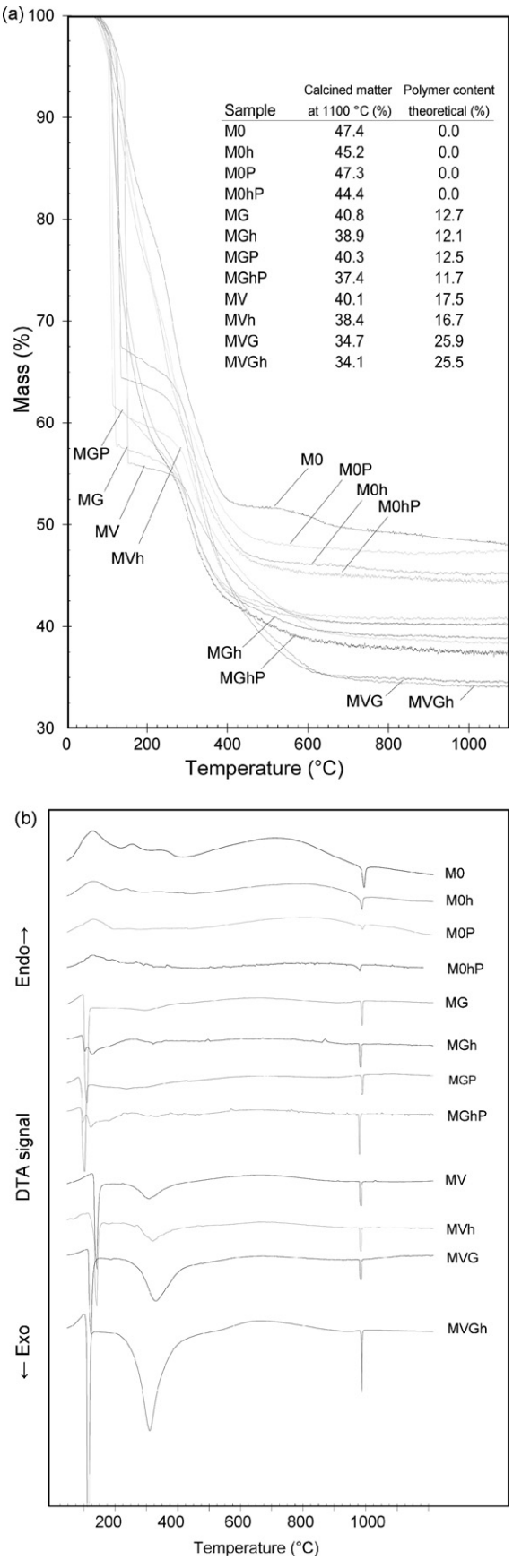

Fig. 4. (a) TG weight loss curves and (b) adjusted DTA curves of gel samples with heating rate of 5 °C min^{-1}.

kind of fast removal of matter has been observed previously with the ANN–TEOS alcogels,[2,41] attributed mainly to the volatilisation of water, but also to the carbon and nitrogen containing species,[2] such as unhydrolysed alkoxy-groups and nitrous gases. Consequently, for the gels containing no polymer, the amount of residual matter after 200 °C was almost ∼30%, whereas for the polymer containing gels (excluding the theoretical content of the added polymers), it was less than 5% (PEG–HCl-containing gels ∼10%). The decomposition of PEG and PVP was evident above 250–280 °C,[19–21,42] together with the obvious condensation of inorganics, as the dehydroxylation and the irreversible collapse of the PI/A-like structure typically occurs at 250–500 °C.[43–46] Above 700 °C, the mass losses were lower. No mass loss step at 1000 °C was observed, which indicates that mullite crystallized mostly through structural re-arrangements in an amorphous phase.[39,40] It has been shown that in Type I gels, the release of residual carbon and nitrates[14,40] or water from OH recombination[9,47] occur at temperatures higher than expected, due to the entrapment of these species in micropores or closed pores.[47] However, the amount of residual matter in our nanoparticulate Type I gel was still less than in a typical Type I gel at 700–900 °C,[47] and the matter released by the crystallization was hardly detectable for M0 at 1000 °C.

In DTA (Fig. 4b), M0 displayed the highest endothermic reaction related to the water removal at 100–400 °C, which implies that the changes during the dehydration influenced the yield of mullite at 900 °C. The second weaker endotherm at 400–900 °C might be associated with the release of entrapped residuals. For the polymer containing gels, in contrast, the first broad endotherm was suppressed either by one pronounced and sharp exotherm, or by two smaller ones at 110–160 °C. Moreover, for PVP-containing gels, a second, broad exotherm was observed at 280–350 °C, which was very intense for MVGh. The sharp exotherm coincidences with the mass loss observed in TG, and may therefore be assigned to the removal of physical water, solvents and nitrous gases, which, however, are typical endothermic processes.[2,48,49] As the azeotropic temperature for water/nitric acid mixture (68 wt.%) of 120.5 °C is reached, nitric acid was obviously concentrated. Consequently, the sharp exotherm may be connected to a catalysed oxidation of the solvents/polymer by the concentrated nitric acid, such as very fast aldehyde and ketone reaction of primary and secondary alcohols, respectively, and the reaction products could have been evaporated simultaneously due to their lower boiling point (except in the case of oxidised PEG). The broad exotherm at 320 °C in DTA, with the prominent weight loss found in TG, reconciles with the decomposition of organics species, likely in combination with a partial dehydroxylation and PI/A structural collapse. Also, in the presence of organic substances with synthetic hydroxyaluminosilicates at around 300 °C,[50] some exothermic formation of an intermediate allophane configuration with $Al(OH)_3$(s) cannot be ruled out. As the exotherm at 320 °C was pronounced with the gels exhibiting the spinel phase, the structural changes towards the spinel phase formation might have took place during or before the dehydroxylation of PI/A-like units and the decomposition of organics.

At 977–995 °C, a distinct exotherm ascribed to typical mullitization of Type I precursor[7–11] was observed, appearing much sharper for the polymer-containing gels, especially for MGhP and MVGh. Usually, the crystallization of spinel phase yields a weak DTA signal,[5,52] however, despite the presence of the spinel phase, the DTA data of MVGh unexpectedly show that the crystallization exotherm at around 980 °C is sharp and strong.

3.4. Densification of gels

Densification curves measured during heat treatment are shown in Fig. 5. At temperatures below 400 °C, the densification of gels void of polymer can be ascribed to polymerisation of inorganics,[37] while viscous flow sintering occurred in the temperature range of 450–970 °C. As an exception, viscous flow sintering took already place for M0 at 400–550 °C, followed by a region with a zero slope of shrinkage at 600–900 °C. Prior to mullite crystallization, a slight shrinkage was observed at 900–1000 °C. For the polymer-containing gels, apparent organics removal (shrinkage and mass loss) continued until 650 °C (for MV, the rapid shrinkage at 140 °C associates with the fast removal of volatile matter), and steady sintering occurred at 700–900 °C. Prior to mullite crystallization, an opulent densification at 900–1000 °C was observed. For gels with the highest shrinkage, a small shoulder in the curve just at the end of the opulent section was observed. The final linear shrinkages of the PVP–PEG containing gels were as high as 41%, which can be compared to 24% for M0.

For M0, densification at 900–1000 °C was small, whereas for M0h, a more pronounced shrinkage was observed. This suggests that the particles in M0h gel are less tightly packed, which may associate with the lower mullite crystallinity at 900 °C. For the amorphous gels that showed the opulent densification just before crystallization, the nucleation sites for mullite were likely formed during it. The additional shoulder may relate on a relaxation after final rearrangements.[37,40] Although the spinel phase forming gel exhibited pronounced re-arrangements during heat treatment, the opulent section was even more pronounced for MV and MVh, which both showed only mullite in XRD. Gels that contained 1-PrOH could not be characterized by dilatometry due to their low mechanical strength.

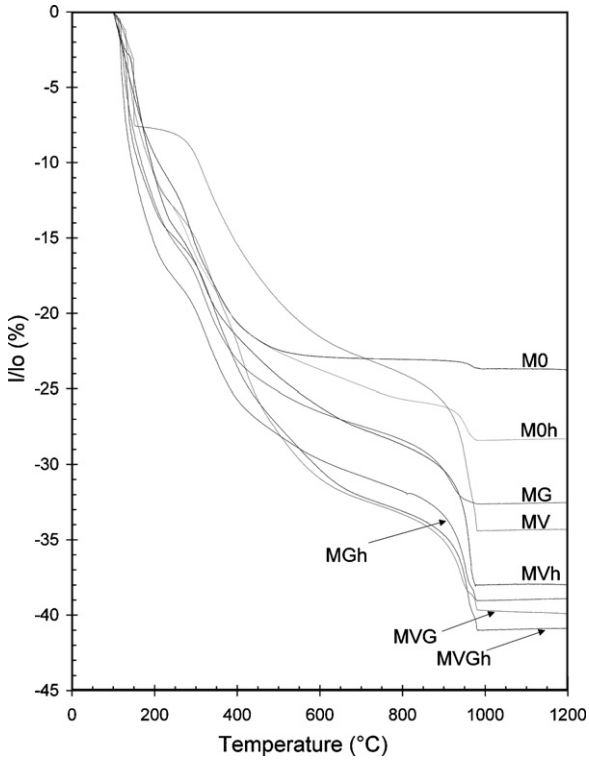

Fig. 5. Dilatometer curves with heating rate of 5 °C min^{-1}.

3.5. Evolution of the pore characteristics

N_2 sorption isotherms measured for the different materials after heat treatment at different temperatures are shown in Fig. 6,

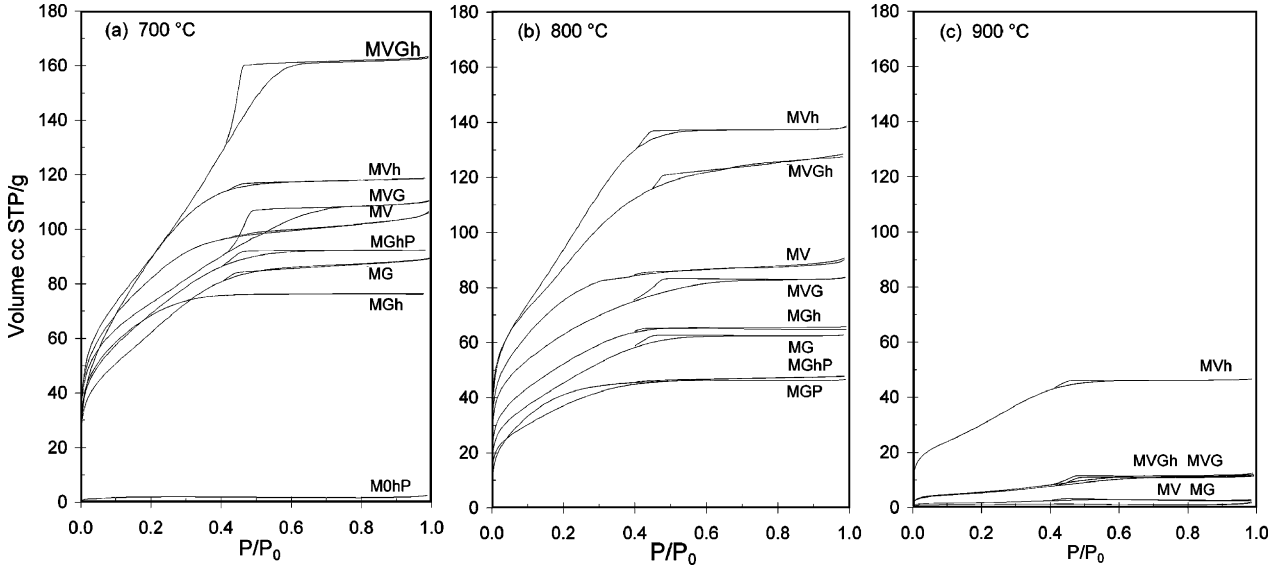

Fig. 6. N_2 adsorption–desorption isotherms for gels heat-treated with heating rate of 5 °C min^{-1} for 1 h at (a) 700 °C, (b) 800 °C and (c) 900 °C.

Table 3
Physisorption data for gels heat-treated for 1 h at 700 °C, 800 °C and 900 °C

Abbreviation	700 °C			800 °C			900 °C		
	SSA (m^2/g)	V_{micro} (ml/g)	V_{meso} (ml/g)	SSA (m^2/g)	V_{micro} (ml/g)	V_{meso} (ml/g)	SSA (m^2/g)	V_{micro} (ml/g)	V_{meso} (ml/g)
Sols									
M0	<2	–	–	<2	–	–	<2	–	–
MG	230.9	0.137	0.025	168.0	0.097	0.016	6.2	0.005	0.002
MV	296.4	0.150	0.022	270.0	0.141	0.012	3.7	0.001	0.000
MVG	257.4	0.168	0.066	223.1	0.127	0.027	19.6	0.016	0.011
With HCl									
M0h	<2	–	–	<2	–	–	<2	–	–
MGh	240.7	0.119	0.001	190.0	0.102	0.004	<2	–	–
MVh	347.9	0.182	0.018	361.1	0.213	0.028	115.5	0.072	0.010
MVGh	335.9	0.249	0.119	320.9	0.202	0.059	20.6	0.017	0.011
With 1-PrOH									
M0P	<2	–	–	<2	–	–	<2	–	–
MGP	<2	–	–	136.8	0.072	0.006	<2	–	–
With HCl and 1-PrOH									
M0hP	6.4	0.002	0.000	<2	–	–	<2	–	–
MGhP	251.7	0.143	0.020	152.1	0.072	0.005	<2	–	–

SSA is measured from the adsorption branch P/P_0 0.05–0.25 by using the BET theory. V_{micro} is externally measured from the second linear region of the *t*-plot in the range of 0.8–1.5 nm. V_{meso} is measured from the desorption branch by using the BJH method.

and the derived parameters are summarized in Table 3. The surface areas of gels void of polymer were very low after heat treatments at 700–900 °C, with specific surface areas <2 m^2/g, with M0hP as a slight exception. The absence of porosity in these gels is in good agreement with the dilatometry results, where more than 90% of the densification had occurred already at temperatures below 700 °C. For the polymer-containing gels calcined at 700 °C, in contrast, the SSAs were between 231 and 296 m^2/g (MGP as an exception), and in the presence of HCl, the SSAs were even higher, 241–348 m^2/g. The SSAs were normally lower after heat treatment at 800 °C as compared to materials treated at 700 °C, while the opposite was observed for MGP and MVh. However, for all gels originally containing polymer, the surface areas were lower after heat treatment at 900 °C, as compared to the SSAs measured after heat treatment at 700 °C or 800 °C, being in good agreement with the DTA/TG and dilatometry results. Moreover, the SSAs at 700 °C or 800 °C were generally high with the gels being X-ray amorphous at 900 °C, which again connects the low SSA to the early formation of the mullite nucleation sites in the gels void of polymers, especially in M0. In single-phase ANN–TEOS alcogels, high SSAs are sometimes reported even after mullite formation.[53] The SSA reduction in our gels implies a partial presence of the viscous phase in the aluminosilicate matrix (likely with a very fine particle size in the nanometre length scale).

At 700–800 °C, the polymer-containing gels were generally microporous, and for the PVP–PEG gels a clear uptake in the relative pressure range $P/P_0 = 0.4$–0.6 was present, due to capillary condensation in mesopores (Fig. 6a). At 900 °C, most of the gels originally containing polymer were non-porous, but MVh, MVG and MVGh still showed some porosity. The highest mesopore volumes were observed for the spinel forming gels. The presence of mesopores can be attributed to interparticulate porosity,[1,37,54] arising from the segregating effect of polymers and chloride. For gels containing no polymer, the mullite crystallization at 900 °C may be explained, again, as the early formation of mullite nucleation sites in dense structures below 900 °C, while for the more porous structure of the polymer-containing gels, larger volumetric changes by diffusion, as observed with the opulent step in dilatometer, were required for the nucleation-growth of mullite. This suggests that the diffusion of silica was needed in order to induce mullite nucleation, implying also that the mesoporosity may be connected to the presence of free silica. Thus, the formation of spinel phase might be a consequence of the lack of the necessary structural arrangements to receive a mullite-favouring order. This is especially true at heat-treatment temperatures of 900 °C, which is close to the plausible immiscibility region[55] where the mobility of silica should be high. This likewise implies distributed particle size in gels containing spinel phase; due to the isolation by polymers, some part of the particles may have remained below the critical size of mullite nucleus of about 10 nm,[8] but some closer to the one of transitional alumina known to be much less at about 3 nm.

3.6. Structural evolution during the heat treatment

Selected FTIR spectra of gels are shown in Fig. 7a and the corresponding assignments[5,14,42,47,56–67] are listed in Tables 4 and 5. The spectra of dried gels are similar to those reported for natural and synthetic proto-imogolite allophane,[14,45,58–60] with two characteristic broad adsorption bands in the range of 500–680 cm^{-1} assigned to Al–O stretch in AlO_6 units and in the range of 900–1200 cm^{-1} assigned to Si–OH bending vibrations as well as to stretching vibrations of Si–O–Si and Si–O–Al. Importantly, absorption bands that could be assigned to amorphous silica at 800 cm^{-1},[60] or to Al–O–Al linkages in AlO_4 units at 840–870 cm^{-1} were not detected. Thus, the FTIR results are in good

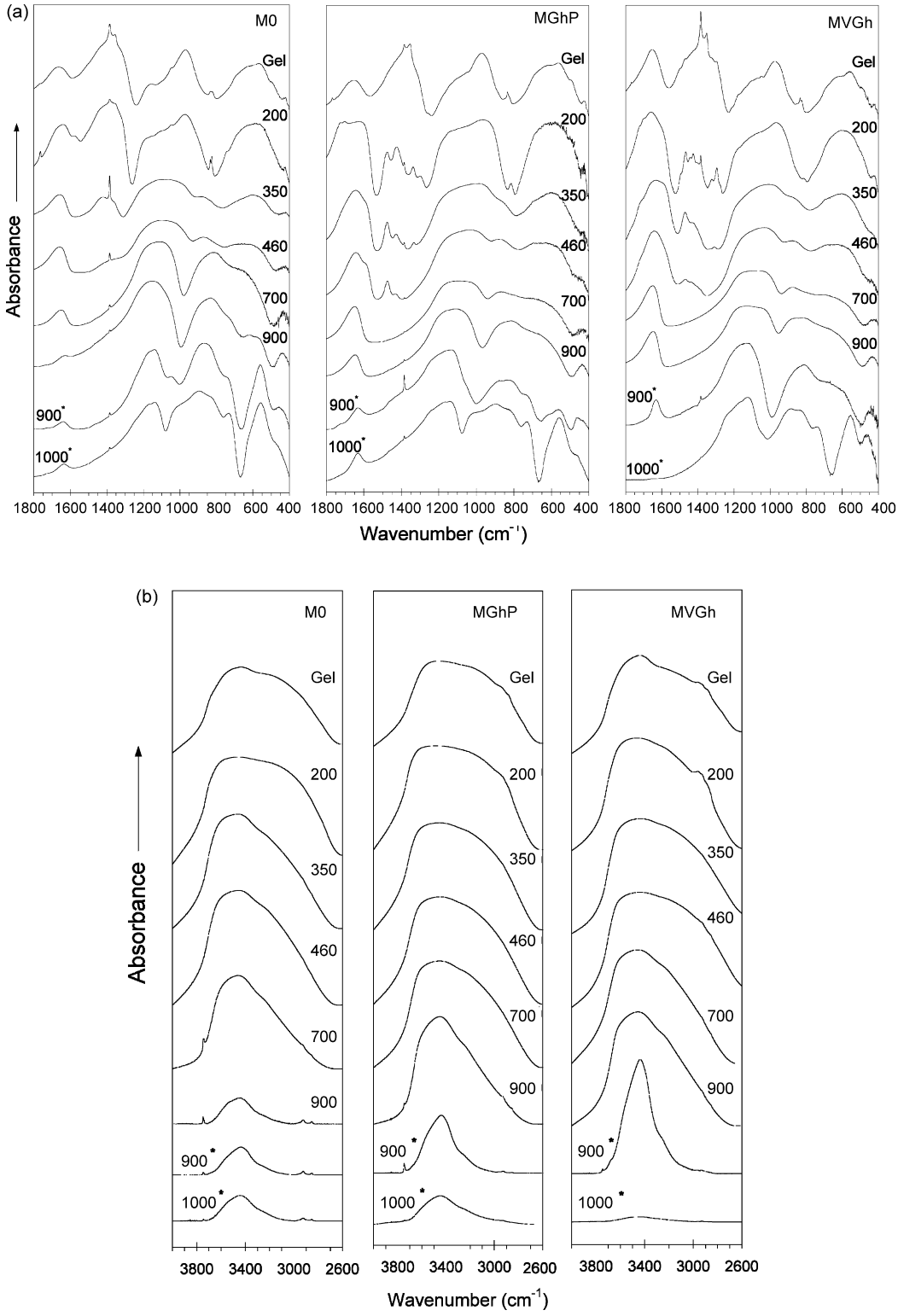

Fig. 7. FTIR spectra in the region (a) 400–1800 cm^{-1} and (b) 2600–4000 cm^{-1} of heat-treated (discrete) gel samples of M0, MGhP and MVGh as a function of heat treatment temperature. Gel indicates the dry gel and numbers the gels that were heat-treated with a heating rate of 5 °C min^{-1} at respective temperatures of 200–1000 °C. The heat-treated gels were not subjected to any isothermal dwell, except the gels that were marked with an asterisk and treated at 900 °C and 1000 °C for 1 h.

agreement with the solid-state NMR results. The broad overlapping absorption bands in the region 1230–1500 cm^{-1} are assigned to CH bending vibrations in the used solvents, unhydrolysed species and organic polymers, as well as to ionic NO_3^-. At higher wavenumbers (Fig. 7b), CH stretching vibrations (~2800–3000 cm^{-1})[42,56] and OH stretching vibrations (~2900–3600 cm^{-1})[47] created a broad envelope of absorbances.

Table 4
FTIR absorbance band assignments in the region of 400–1800 cm^{-1} for aluminosilicate gels containing polymers and non-crystalline matter

No polymer (cm^{-1})	PEG-added (cm^{-1})	PVP-added (cm^{-1})	Assignment[5,14,42,47,56–68]
1766			
	1713		C=O stretch[56]
	1692		
		1715	amide[42,56]
		1690	C=O<, C–N stretch[42,56]
1640–1600	1640–1600	1640–1600	H_2O bend[56,57]
~1550	~1550	~1550	unidentified, (AlO_4•OH_2^+ related?)[58]
		1485	C–N[42,56]
1466	1466	1464	CH_2 scissor[42,56]
		1434	
1417	1417	1421	asym CH_3 bend[56]
		1393	CH bend (in PVP)[42]
1384	1384	1384	ionic NO_3^- stretch,[14,63] sym CH_3 bend[56]
1347	1351	1351	C-H bend doublet in *gem*-dimethyl[56], distorted ionic NO_3^- stretch[63]
	1330		
1313		1312	CH_2 wag, C–N stretch[42,56]
	1292	1292	
	1244		sym C–O–C stretch[56]
~1220	~1220	~1220	asym Si–O–Si stretch (aluminosilicates, LO mode SiO_2),[57,61] CH_2 twist[42,56]
~1160	~1160	~1160	asym Si–O–Si stretch (aluminosilicates),[61] Al–OH bend (alumina gel)[65]
~1130	~1130	~1130	asym Si–O–Si stretch (aluminosilicates),[61]
~1100	~1100	~1100	asym Si–O–Si stretch TO mode (SiO_2),[57,66]
~1090	~1090	~1090	Si–O–C stretch[57]
~1080	~1080	~1080	Si–O–Si resembling strecth of Si(O–Al_3) (imogolite)[68]
~1050	~1050	~1050	ionic NO_3^- stretch,[63] Al–OH bend (alumina gel)[65]
~1040	~1040	~1040	asym C–O–C stretch[56]
970~1080	970~1080	970~1080	Si–O–T (T = AlO_4 or SiO_4) stretch,[5,59,61,62,65] Al–OH–Al[65]
~940–990	~940–990	~940–990	Si–OH bend,[58] Si–O$^-$$R^+$ stretch[61]
~940	~940	~940	Si–O–Al (AlO_6) stretch in imogolite[68]
814–885	809–887	808–883	Al–O stretch AlO_4 units[47,66]
833	833	833	ionic NO^{3-} stretch[63]
821–824	810–824	810–824	Al–OH bend (in imogolite)[58,59]
796	800–810	804–813	sym Si–O–Si stretch (SiO_2)[60,57]
742–749			T–O–T bend (TO_4)[47]
726			ionic NO^{3-} stretch[63]
500–680	500–680	500–680	Al–O and Al–O–T stretch, AlO_6 units[47,64,65]
		580–650	N–C=O bend ring deformation[42]
~570	~570	~570	O–Si–O stretch in imogolite[68]
~490	~490	~490	Al–OH stretch in imogolite[68]
419–448	422–435	420–440	Si–O–Si bend (SiO_2)[57,61]

For gels heat-treated at 200 °C (Fig. 8a), a clear decrease in the doublet geminal dimethyl absorbance of the isopropoxy group (1350–1400 cm^{-1}) was observed for each polymer-containing gel, which may be connected to the removal of 2-propanol (by-product from AIP hydrolysis, unhydrolysed species in PI/A units). For distorted nitrate ion, a splitting at 1348 cm^{-1} is also reported,[63] whereas the remaining peak at 1384 cm^{-1} is assigned to free ionic nitrate.[14,63] As the adsorption bands ascribed to characteristic groups in PEG (CH_2 and C–O–C) and PVP (CH_2, C=O and CN) were still present after treatment at 200 °C, it is thus obvious that the rapid exotherms at 110–160 °C are more connected to the removal of the organic solvents and unhydrolysed groups (and partially also to nitrous species), which can also be linked with the high SSAs and fairly small micropore volumes. For M0, in contrast, the adsorption bands for these species remained almost unchanged. It is known that the natural PI/A resembling phases may begin their dehydroxylation already at temperatures of 155–200 °C,[45,46] which, however, seems not yet likely to occur herein, due to the strong presence of Si–OH (and Al–OH) adsorption bands in the gels

Table 5
FTIR absorbance band assignments for gels with mullite

No polymer (cm^{-1})	PEG-added (cm^{-1})	PVP-added (cm^{-1})	Assignments mullite after Voll et al.[67]
1161	1172	1167	Si–O stretch (SiO_4), in-plane
1131	1132	1124	Si–O stretch (SiO_4), in-plane
	1034	1060	(see Table 4)
1004	975	968	Si–O stretch (SiO_4), out-of-plane
894	899	885	Al–O stretch (AlO_4), out-of-plane
822	820	833	Al–O stretch (AlO_4), in-plane
734	740	739	T–O–T bend (TO_4), in-plane
626	624	624	O–Al–O bend (AlO_4)
556	555	554	Al–O stretch (AlO_6)
477	470	473	Al–O–Al bend (AlO_6) and O–Si–O bend (SiO_4)
		425	(see Table 4)

still after heat-treatment at 200 °C. The C=O bond appearance with PEG is also noteworthy, since this supports the possible oxidation reaction of alcohols and PEG, probably catalysed by nitric acid. Moreover, it should be noted that the band appearing at ~1100 cm^{-1}, especially in the mesoporous gels, can be ascribed to Si–O–Si linkages of amorphous SiO_2 (as well as to Si–O–C).[5,47,57,66] The early presence of this adsorption band implies that during the fast removal of the matter, structural changes in the nanoparticulate matter occurred, due to the condensation and residual alcohol removal, and some phase separation of silica microdomains (with organics) might have then occurred.[22]

At 350 °C (see Fig. 8b), the combustion of the polymers evolved due to the decrease of CH-related vibrations. It is clear that there is still a certain amount of organics and nitrates left in gels void of polymer. Also, the structural breakdown of the PI/A seems to be underway, as the absorption band near 840–870 cm^{-1} for AlO_4 emerged. For PI/A structures, as well as for homogeneous mullite gels, the Al coordination is usually modified due to the dehydroxylation,[10,15,22,51,52,58,69] and according to Jaymes et al.,[12–15] the portion of AlO_4 and AlO_5 (AlO_5 associates with triclustered AlO_4 species having T^*O_4 and TO_4 connections)[10] should increase as a function of the heat treatment temperature. Equally, the plausible Si–O–Al vibra-

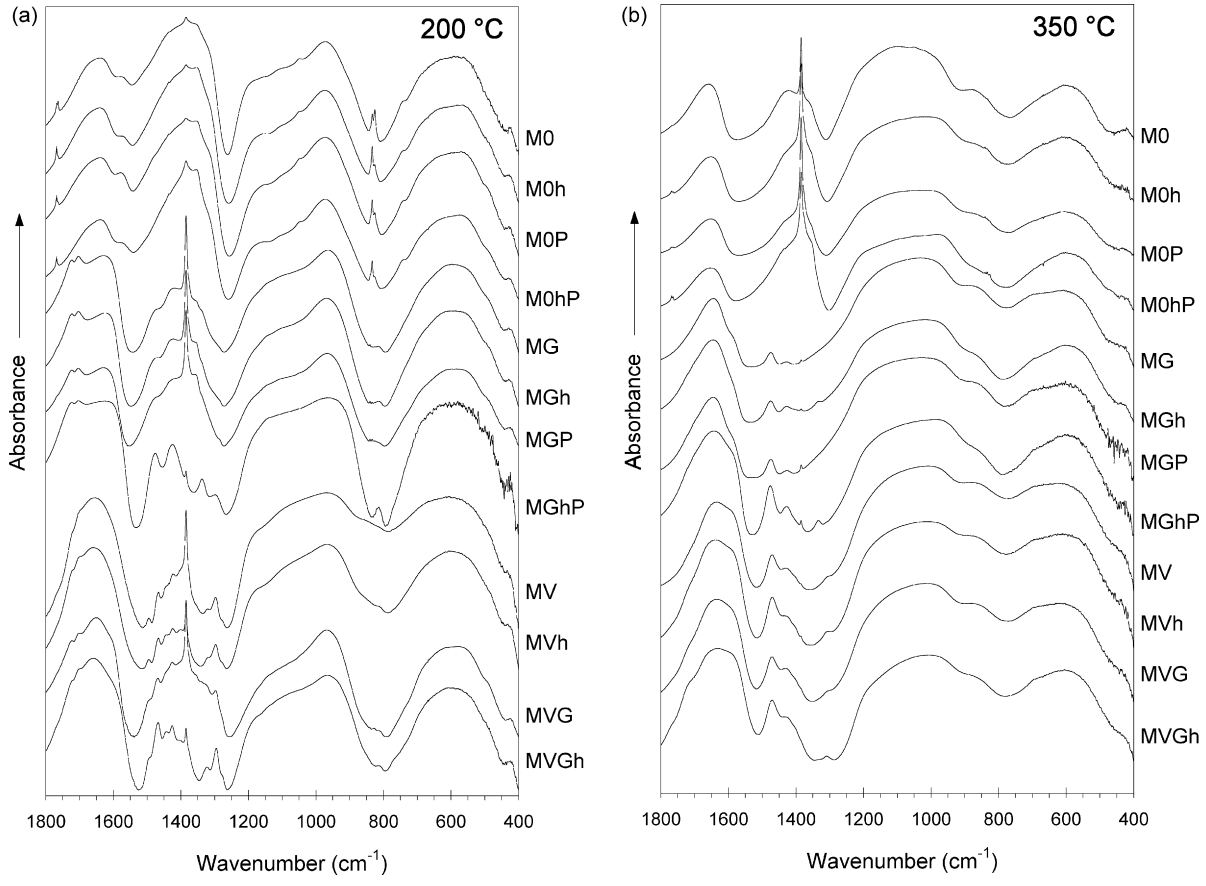

Fig. 8. FTIR spectra of the gels in the region 400–1800 cm^{-1} heat-treated with a heating rate of 5 °C min^{-1} at (a) 200 °C and (b) at 350 °C.

tions (of AlO_6) in imogolite[68] at ~940 cm^{-1} were diminished (especially for M0), and the Si–OH stretches at 950–970 cm^{-1} were shifted to higher wavenumbers, indicating the formation of an amorphous aluminosilicate network as well.[58,70] For MV, the absorbance at 850–900 cm^{-1} was observed already at 200 °C, which suggests, together with the dilatometry results, that when plain PVP was used, the interparticulate surface reactions differed or were delayed during the alkoxy-group removal, which supports the microphase separation in the presence of both polymers and HCl. In this light, the most evident band at ~1100 cm^{-1} for M0, together with the ~440 cm^{-1} adsorption, seems a bit surprising, which suggests silica (or Si–O–C)[22] formation also in the gels not containing polymer at 350 °C.

At 460 °C (see Fig. 7a), the mutual differences between spectra recorded for the different gels were minor. It nevertheless confirms the DTA/TG and dilatometry results that the major part of the dehydroxylation of PI/A units occurred in the range of 200–460 °C, perhaps mostly in the range of 200–350 °C.

Upon further heating at 700 °C, the Si–O–Al vibrations gradually shifted to higher values. At 700 °C, the absorption bands near 840–870 cm^{-1} (AlO_4) and 540–600 cm^{-1} (AlO_6) were clearly evolved and sharp for M0, while for the others, these were still fairly broad. This may now indicate that when the structure was denser, as observed with TG, dilatometry and gas adsorption, PI/A-like structure collapse and dehydroxylation results in higher structural order, which favours the early formation of mullite nuclei. This is also supported by the new band appearing in the region 720–740 cm^{-1}, attributed to TO_4 units,[47,67] that are known to act as nucleation sites for mullite.[8–11,51] Thus, this view is in good agreement with the literature for the dehydroxylation of natural phases[43,44,70] and the structural evolution of synthetic PI/A precursors,[12–15] as well as with our results showing that after the PI/A structure collapsed, sintered and non-porous structure was soon developed in M0. Moreover, M0 behaved like Type I gel[47] losing its strong H-bonded species of OH (3230 cm^{-1}) and H_2O (2960 cm^{-1}) after the dehydroxylation (see Fig. 7b). In contrast, the polymer-containing gels, especially MVGh, showed more like Type III gel behaviour with H-bonded water, up to 700 °C. For these gels, FTIR revealed that the carbon from the decomposition of polymers likely shielded the nanoparticulate structure over the dehydroxylation step, although the solvents and/or unhydrolysed alkoxide groups were removed at the early stages. Consequently, it seems that polymers can prevent the early mullite nucleation, as inferred from the absence of TO_4, causing higher structural disorder and porosity. The mesoporosity may be connected with the silica segregation as well.

At 900 °C (see Fig. 7a), for M0, the alumina absorbances sharpened, whereas for MGhP and MVGh, these showed still a vague envelope. However, for M0, a dwell at 900 °C was still required, in order to obtain crystallinity, as the sample without a dwell was amorphous at 900 °C (data not shown). This clearly shows that the amount of the plausible TO_4 nucleation sites was sustained[51] (or even increased) for M0 during the dwell at 900 °C. The absorbances of physical water were found for each gel. Although the non-H bonded H_2O (~3400 cm^{-1}) may originate from the atmospheric moisture in the porous gels, Beran et al.[47] have showed that the residual hydroxyl recombination can induce the "recombination-produced" water to be trapped water within the (closed or microporous) structure even at such high temperatures. The trapping also supports the presence of nitrate at temperatures higher than expected, which explains the delayed matter removal in the M0 gel.

In crystalline samples, the characteristic bands of mullite[67] became evident (Table 5). Additionally, the absorption at 1020–1060 cm^{-1} was clear for the polymer-containing gels, assigned to the Si–O–T linkages in the residual amorphous aluminosilicate matrix. Furthermore, the SiO_2 vibrations were found for MVGh at ~430 cm^{-1} and ~1100 cm^{-1}, which clearly affirms the partial presence of SiO_2 at 1000 °C. Thus, MVGh shows typical absorption of the spinel phase as well,[71] as was found in XRD. The free silica caused the heterogeneous Al-rich aluminosilicate regions that likely formed spinel phase in MVGh,[16,72] however, these regions being distributed uniformly, as the gel contained mostly monophasic-like mullite after heat treatment at 1000 °C.

4. Conclusions

Non-ionic polymers studied herein can be used as processing aids with the PI/A resembling nanoparticles, importantly, without interfering the Al–O–Si bonding within the particles in the sol–gel state. Even large physical deformations with shrinkages close to 40%, did not lead to non-monophasic crystallization. Thus, the further applicability of the nanoparticulate aluminosilicate/mullite precursor with various structural modifiers was demonstrated, based on the sustained chemical homogeneity of the monophasic-like Type I gel. However, despite the high degree of homogeneity, the presence of the polymer (and the carbon from its decomposition) seemed to hinder the early formation of mullite nuclei at those temperatures where the non-added gel showed the formation. In the polymer-containing gels, transitional mullite was detected when viscous sintering first reduced the porosity in the range of 900–1000 °C. Moreover, an evident co-crystallizing spinel phase was detected in one studied sample, which was linked to a pre-microphase separation where silica species are adsorbed to phase-separated polymer together with Cl^- ions. This has apparently occurred after the removal of the organic by-product solvents and/or residual alkoxy-groups at temperatures close or below the dehydroxylation of the PI/A resembling phase. The preparation of highly (meso)porous monophasic-like aluminosilicates structures with transitional mullite may be successful when the structural arrangements at low temperatures, as well as the powerful densification before mullite crystallization are paid attention to. This information is useful in designing nanostructures from the nanoparticulate precursor to the homogeneous aluminosilicate/mullite ceramics.

Acknowledgements

Authors are grateful to Dr. Bodo Zibrowius, Max-Planck-Institut für Kohlenforschung, Germany for the MAS NMR study.

J.L. appreciates Terhi Hämäläinen, Elena Riipinen, Minna Uusitalo and Leo Hyvärinen for their laboratory assistance in TUT. We also want to thank one of the referees for giving valuable comments on how to improve the manuscript.

References

1. Vendange, V. and Colomban, Ph., How to tailor the porous structure of alumina and aluminosilicate gels and glasses. *J. Mater. Res.*, 1996, **11**, 518–528.
2. Sinkó, K. and Pöppl, L., Transformation of aluminosilicate wet gel to solid state. *J. Solid State Chem.*, 2002, **165**, 111–118.
3. Verdenelli, M., Parola, S., Chassagneux, F., Létoffé, J.-M., Vincent, H., Scharff, J.-P. *et al.*, Sol–gel preparation and thermo-mechanical properties of porous $x Al_2O_3$–$y SiO_2$ coatings on SiC Hi-Nicalon fibres. *J. Eur. Ceram. Soc.*, 2003, **23**, 1207–1213.
4. Leivo, J., Meretoja, V., Vippola, M., Levänen, E., Vallittu, P. and Mäntylä, T. A., Sol–gel derived aluminosilicate coatings on alumina as substrate for osteoblasts. *Acta Biomater.*, 2006, **2**, 659–668.
5. Okada, K. and Otsuka, N., Characterization of the spinel phase from SiO_2–Al_2O_3 xerogels and the formation process of mullite. *J. Am. Ceram. Soc.*, 1986, **69**, 652–656.
6. Nishio, T., Kijima, K., Kajiwara, K. and Fujiki, Y., The influence of preparation procedure in the mullite preparation by solution method to the mixing of Al and Si and the crystallization behavior. *J. Ceram. Soc. Jpn. Int. Ed.*, 1994, **102**, 464–472.
7. Schneider, H., Okada, K. and Pask, J., *Mullite and Mullite Ceramics*. Wiley, Chichester, England, 1994, pp. 122–140.
8. Schneider, H. and Komarneni, S., *Mullite*. Wiley–VCH, Weinheim, Germany, 2005, pp. 93–128, 262–286.
9. Schneider, H., Voll, D., Saruhan, B., Sanz, J., Schrader, G., Rüscher, C. *et al.*, Synthesis and structural characterization of non-crystalline mullite precursors. *J. Non-Cryst. Solids*, 1994, **178**, 262–271.
10. Schmücker, M. and Schneider, H., Structural development of single phase (Type I) mullite gels. *J. Sol–Gel Sci. Technol.*, 1999, **15**, 191–199.
11. Schmücker, M. and Schneider, H., A new approach on the coordination of Al in non-crystalline gels and glasses of the system Al_2O_3–SiO_2. *Ber. Bunsen. Phys. Chem.*, 1996, **100**, 1550–1553.
12. Jaymes, I., Douy, A., Massiot, D. and Busnel, J.-P., Synthesis of a mullite precursor from aluminum nitrate and tetraethoxysilane via aqueous homogeneous precipitation: an ^{27}Al and ^{29}Si liquid- and solid-state NMR spectroscopic study. *J. Am. Ceram. Soc.*, 1995, **78**, 2648–2654.
13. Jaymes, I. and Douy, A., New aqueous mullite precursor synthesis. Structural study by ^{27}Al and ^{29}Si NMR spectroscopy. *J. Eur. Ceram. Soc.*, 1996, **16**, 155–160.
14. Jaymes, I., Caractérisations physico-chimiques de poudres silicates synthétisées par de nouvelles voies sol–gel: application à la mullite. PhD Thesis. University of Orleans, Orleans, France, 1995, pp. 35–45.
15. Jaymes, I., Douy, A., Massiot, D. and Coutures, J. P., Characterization of mono- and diphasic mullite precursor powders prepared by aqueous routes ^{27}Al and ^{29}Si MAS-NMR spectroscopy investigations. *J. Mater. Sci.*, 1996, **31**, 4581–4589.
16. Huling, J. C. and Messing, G. L., Epitactic nucleation of spinel in aluminosilicate gels and its effect on mullite crystallization. *J. Am. Ceram. Soc.*, 1991, **74**, 2374–2381.
17. Leivo, J., Lindén, M., Teixeira, C. V., Puputti, J., Rosenholm, J. M., Levänen, E. *et al.*, Sol–gel synthesis of a nanoparticulate aluminosilicate precursor for homogeneous mullite ceramics. *J. Mater. Res.*, 2006, **21**, 1279–1285.
18. Kozuka, H., Kajimura, M., Hirano, T. and Katayama, K., Crack-free, thick ceramic coating films via non-repetitive dip-coating using polyvinylpyrrolidone as stress-relaxing agent. *J. Sol–Gel Sci. Technol.*, 2000, **19**, 205–209.
19. Kajihara, K. and Yao, T., Macroporous morphology of the titania films prepared by a sol–gel dip-coating method from the system containing poly(ethylene glycol). III. Effect of chemical additives. *J. Sol–Gel Sci. Technol.*, 1999, **16**, 257–266.
20. Kajihara, K. and Nakanishi, K., Macroporous morphology of titania films prepared by a sol–gel dip-coating method from a system containing poly(ethylene glycol) and poly(vinylpyrrolidone). *J. Mater. Res.*, 2001, **16**, 58–66.
21. Yoshida, M. and Prasad, P. N., Sol–gel-processed SiO_2/TiO_2/poly (vinylpyrrolidone) composite materials for optical waveguides. *Chem. Mater.*, 1996, **8**, 235–241.
22. MacKenzie, K. J. D., Meinhold, R. H., Patterson, J. E., Schneider, H., Schmücker, M. and Voll, D., Structural evolution in gel-derived mullite precursors. *J. Eur. Ceram. Soc.*, 1996, **16**, 1299–1308.
23. Mizukami, F., Maeda, K., Toba, M., Sano, T., Niwa, S.-I., Miyazaki, M. *et al.*, Effect of organic ligands used in sol–gel process on the formation of mullite. *J. Sol–Gel Sci. Technol.*, 1997, **8**, 101–106.
24. Lee, J.-E., Kim, J.-W., Lee, J.-H. and Jung, Y.-G., Mullite precursor synthesis in aqueous conditions: dependence of mullite crystallization and grain size and morphology on solution pH and precursor salt. *J. Mater. Res.*, 2004, **19**, 1133–1138.
25. Pereira, M. M. and Hench, L. L., Mechanism of hydroxyapatite formation on porous gel–silica substrates. *J. Sol–Gel Sci. Technol.*, 1996, **7**, 59–68.
26. Peltola, T., Jokinen, M., Rahiala, H., Levänen, E., Rosenholm, J. B., Kangasniemi, I. *et al.*, Calcium phosphate formation on porous sol–gel derived SiO_2 and CaO–P_2O_5–SiO_2 substrates in vitro. *J. Biomed. Mater. Res.*, 1999, **44**, 12–21.
27. Webster, T. J., Ergun, C., Doremus, R. H., Siegel, R. W. and Bizios, R., Enhanced functions of osteoblasts on nanophase ceramics. *Biomaterials*, 2000, **21**, 1803–1810.
28. Sinkó, K., Mezei, R. and Zrínyi, M., Gelation of aluminosilicate systems under different chemical conditions. *J. Sol–Gel Sci. Technol.*, 2001, **21**, 147–156.
29. Okada, K., Yasohama, S., Hayashi, S. and Yasumori, A., Sol–gel systems of mullite long fibres from water solvent systems. *J. Eur. Ceram. Soc.*, 1998, **18**, 1879–1884.
30. Lippens, B. C. and de Boer, J. H., Studies on pore systems in catalysts V. The *t* method. *J. Catal.*, 1965, **4**, 319–323.
31. Barrett, E. P., Joyner, L. G. and Halenda, P. P., The determination of pore volume and area distributions in porous substances I. Computations from nitrogen isotherms. *J. Am. Chem. Soc.*, 1951, **73**, 373–380.
32. Mittelbach, P., Zur roentgenkleinwinkelstreuung verdunter kolloider systeme. VIII. Diskussion des streuverhaltens regelmaessiger koerper und methoden zur bestimmung von groesse und form kolloider teilchen. *Acta Phys. Austriaca*, 1964, **19**, 53–102.
33. Ishiduki, K. and Esumi, K., The effect of pH on adsorption of poly(acrylic acid) and poly(vinylpyrrolidone) on alumina from their binary mixtures. *Langmuir*, 1997, **13**, 1587–1591.
34. Walker Jr., W. J., Reed, J. S., Verma, S. K. and Zirk, W. E., Adsorption behaviour of poly(ethylene glycol) at the solid/liquid interface. *J. Am. Ceram. Soc.*, 1999, **82**, 585–590.
35. Theng, B. K. G., Russell, M., Churchman, G. J. and Parfitt, R. L., Surface properties of allophane, halloysite, and imogolite. *Clays Clay Miner.*, 1982, **30**, 143–149.
36. Adachi, Y., Koga, S., Kobayashi, M. and Inada, M., Study of colloidal stability of allophane dispersion by dynamic light scattering. *Colloid Surf. A*, 2005, **265**, 149–154.
37. Brinker, C. J. and Scherer, G. W., *Sol–Gel Science*. Academic Press, San Diego, CA, 1990, pp. 108, 519–586.
38. Ban, T., Hayashi, S., Yasumori, A. and Okada, K., Characterization of low temperature mullitization. *J. Eur. Ceram. Soc.*, 1996, **16**, 127–132.
39. Okada, K., Activation energy of mullitization from various starting materials. *J. Eur. Ceram. Soc.*, 2008, **28**, 377–382.
40. Douy, A., Crystallization of amorphous spray-dried precursors in the Al_2O_3–SiO_2 system. *J. Eur. Ceram. Soc.*, 2006, **26**, 1447–1454.
41. Cassidy, D. J., Woolfrey, J. L., Bartlett, J. R. and Ben-Nissan, B., The effect of precursor chemistry on the crystallization and densification of sol–gel derived mullite gels and powders. *J. Sol–Gel Sci. Technol.*, 1997, **10**, 19–30.
42. Borodko, Y., Habas, S. E., Koebel, M., Yang, P., Frei, H. and Somorjai, G. A., Probing the interaction of poly(vinylpyrrolidone) with platinum nanocrystals by UV–Raman and FTIR. *J. Phys. Chem. B*, 2006, **110**, 23052–23059.

43. MacKenzie, K. J. D., Bowden, M. E. and Meinhold, R. E., The structure and thermal transformations of allophanes studied by ^{29}Si and ^{27}Al high resolution solid-state NMR. *Clays Clay Miner.*, 1991, **39**, 337–346.
44. MacKenzie, K. J. D., Bowden, M. E., Brown, I. W. M. and Meinhold, R. E., Structure and thermal transformations of imogolite studied by ^{29}Si and ^{27}Al high resolution solid-state nuclear magnetic resonance. *Clays Clay Miner.*, 1989, **37**, 317–324.
45. Farmer, V. C., Adams, M. J., Fraser, A. R. and Palmieri, F., Synthetic imogolite: properties, synthesis, and possible applications. *Clay Miner.*, 1983, **18**, 459–472.
46. Wilson, M. A., Wada, K., Wada, S. I. and Kakuto, Y., Thermal transformations of synthetic allophane and imogolite as revealed by nuclear magnetic resonance. *Clay Miner.*, 1988, **23**, 175–190.
47. Beran, A., Voll, D. and Schneider, H., Dehydration and structural development of mullite precursors: an FTIR spectroscopic study. *J. Eur. Ceram. Soc.*, 2001, **21**, 2479–2485.
48. Smirnov, L. P. and Summanen, E. V., Rate oscillations in the thermal decomposition of aqueous solutions of nitric acid. *Dokl. Phys. Chem.*, 2002, **386**, 232–234.
49. Feldstein, M. M., Kuptsov, S. A., Shandryuk, G. A., Platé, N. A. and Chalykh, A. E., Coherence of thermal transitions in poly(*N*-vinyl pyrrolidone)–poly(ethylene glycol) compatible blends. 3. Impact of sorbed water upon phase behaviour. *Polymer*, 2000, **41**, 5349–5359.
50. Strekopytov, S. and Exley, C., Thermal analyses of aluminium hydroxide and hydroxyaluminosilicates. *Polyhedron*, 2006, **25**, 1707–1713.
51. Taylor, A. and Holland, M., Chemical synthesis and crystallization of mullite. *J. Non-Cryst. Solids*, 1993, **152**, 1–17.
52. Sanz, J., Sobrados, I., Cavalieri, A. L., Pena, P., de Aza, S. and Moya, J. S., Structural changes induced on mullite precursors by thermal treatment: a ^{27}Al MAS-NMR investigation. *J. Am. Ceram. Soc.*, 1991, **74**, 2398–2403.
53. Li, D. X. and Thomson, W. J., Mullite formation kinetics of a single-phase gel. *J. Am. Ceram. Soc.*, 1990, **73**, 964–969.
54. Sing, K. S. W., Everett, D. H., Haul, R. A. W., Moscou, L., Pierotti, R. A., Rouquerol, J. *et al.*, Reporting physisorption data for gas/solid systems. *Pure Appl. Chem.*, 1985, **57**, 603–619.
55. Takei, T., Kameshima, Y., Yasumori, A. and Okada, K., Calculation of metastable immiscibility region in the Al_2O_3–SiO_2 system using molecular dynamics simulation. *J. Mater. Res.*, 2000, **15**, 186–193.
56. Silverstein, R. M. and Webster, F. X., *Infrared Spectrometry in Spectrometric Identification of Organic Compounds* (*6th ed.*). John Wiley and Sons, New York, 1998, pp. 71–111.
57. Parrill, T. M., Transmission infrared study of acid-catalyzed sol–gel silica coatings during room ambient drying. *J. Mater. Res.*, 1992, **7**, 2230–2239.
58. Parfitt, R. L. and Henmi, T., Structure of some allophanes from New Zealand. *Clays Clay Miner.*, 1980, **28**, 295–302.
59. Cradwick, P. D. G., Farmer, V. C., Russell, J. D., Masson, C. R., Wada, K. and Yoshinaga, N., Imogolite, a hydrated aluminium silicate of tubular structure. *Nat. Phys. Sci.*, 1972, **240**, 187–189.
60. Farmer, V. C., Fraser, A. R. and Tait, J. M., Characterization of the chemical structures of natural and synthetic aluminosilicate gels and sols by infrared spectroscopy. *Geochem. Cosmochem.*, 1979, **43**, 1417–1420.
61. Lee, W. K. W. and van Deventer, J. S. J., Use of infrared spectroscopy to study geopolymerization of heterogeneous amorphous aluminosilicates. *Langmuir*, 2003, **19**, 8726–8734.
62. Rahier, H., Simons, W., van Mele, B. and Biesemans, M., Low-temperature synthesized aluminosilicate glasses. *J. Mater. Sci.*, 1997, **32**, 2237–2247.
63. Vivekanandan, K., Selvasekarapandian, S. and Kolandaivel, P., Raman and FT–IR studies of $Pb_4(NO_3)_2(PO_4)_2{\cdot}2H_2O$ crystal. *Mater. Chem. Phys.*, 1995, **39**, 284–289.
64. Tarte, P., Infrared spectra of inorganic aluminates and characteristic vibrational frequencies of AlO_4 tetrahedra and AlO_6 octahedra. *Spectrochim. Acta A*, 1967, **23**, 2127–2143.
65. Sinkó, K., Mezei, R., Rohonczy, J. and Fratzl, P., Gel structures containing Al(III). *Langmuir*, 1999, **15**, 6631–6636.
66. Kansal, P., Laine, R. M. and Babonneau, F., A processable mullite precursor prepared by reacting silica and aluminum hydroxide with triethanolamine in ethylene glycol: structural evolution and pyrolysis. *J. Am. Ceram. Soc.*, 1997, **80**, 2597–2606.
67. Voll, D., Angerer, P., Beran, A. and Schneider, H., A new assignment of IR vibrational modes in mullite. *Vibr. Spectrosc.*, 2002, **30**, 237–243.
68. McCutcheon, A., Hu, J., Kamali Kannangara, G. S., Wilson, M. A. and Reddy, N., ^{29}Si labelled nanoaluminosilicate imogolite. *J. Non-Cryst. Solids*, 2005, **351**, 1967–1972.
69. Gerardin, C., Sundaresan, S., Benzinger, J. and Navrotsky, A., Structural investigation and energetics of mullite formation from sol–gel precursors. *Chem. Mater.*, 1994, **6**, 160–170.
70. Henmi, T., Tange, K., Minagawa, T. and Yoshinaga, N., Effect of SiO_2/Al_2O_3 ratio on the thermal reactions of allophane. II. Infrared and X-ray powder diffraction data. *Clays Clay Miner.*, 1981, **29**, 124–128.
71. Jin, X.-H., Gao, L. and Guo, J.-K., The structural change of diphasic mullite gel studied by XRD and IR spectrum analysis. *J. Eur. Ceram. Soc.*, 2002, **22**, 1307–1311.
72. Huling, J. C. and Messing, G. L., Chemistry—crystallization relations in molecular mullite gels. *J. Non-Cryst. Solids*, 1992, **147/148**, 213–221.